Immunity
Resource

Cytometry by Time-of-Flight Shows Combinatorial Cytokine Expression and Virus-Specific Cell Niches within a Continuum of CD8+ T Cell Phenotypes

Evan W. Newell,[1] Natalia Sigal,[2] Sean C. Bendall,[1] Garry P. Nolan,[1,2] and Mark M. Davis[1,2,3,*]
[1]Department of Microbiology and Immunology
[2]Institute for Immunity, Transplantation and Infection
[3]The Howard Hughes Medical Institute
Stanford University, Stanford, CA 94305, USA
*Correspondence: mmdavis@stanford.edu
DOI 10.1016/j.immuni.2012.01.002

SUMMARY

Cytotoxic CD8+ T lymphocytes directly kill infected or aberrant cells and secrete proinflammatory cytokines. By using metal-labeled probes and mass spectrometric analysis (cytometry by time-of-flight, or CyTOF) of human CD8+ T cells, we analyzed the expression of many more proteins than previously possible with fluorescent labels, including surface markers, cytokines, and antigen specificity with modified peptide-MHC tetramers. With 3-dimensional principal component analysis (3D-PCA) to display phenotypic diversity, we observed a relatively uniform pattern of variation in all subjects tested, highlighting the interrelatedness of previously described subsets and the continuous nature of CD8+ T cell differentiation. These data also showed much greater complexity in the CD8+ T cell compartment than previously appreciated, including a nearly combinatorial pattern of cytokine expression, with distinct niches occupied by virus-specific cells. This large degree of functional diversity even between cells with the same specificity gives CD8+ T cells a remarkable degree of flexibility in responding to pathogens.

INTRODUCTION

Antigen-specific CD8+ cytotoxic T cells act to clear the body of aberrant or infected cells by recognizing and responding to cognate antigen presented by MHC class I molecules. At any given time, a mixture of CD8+ T cells with a range of antigen experience is circulating throughout the body. Because each of these cells is also exquisitely specific for a very small subset of peptide antigens, an ability to probe the status of cells specific for a given antigen, either by stimulation with antigen or by direct identification with peptide-MHC multimers (Altman et al., 1996; Davis et al., 2011), allows insight into the status of the response to that antigen. Furthermore, landmark studies of the correlation between surface marker phenotypes and overall functional capacity have identified reliable markers for antigen-naive and multiple subsets of antigen-exposed memory CD8+ T cells. That is, based on the average proliferative potential, cytotoxicity and the ability to produce cytokines, naive (CCR7+ CD45RA+), central memory (Tcm, CCR7+CD45RA−), effector memory (Tem, CCR7−CD45RA−), and terminal effector (Teff, CCR7−CD45RA+) cell subsets have been defined (Hamann et al., 1997; Sallusto et al., 1999). Additional CD8+ T cell diversity was found in studies aimed at understanding long-lived memory versus short-lived effector cell fate decisions made by T cells responding to acute infection. IL-7R-expressing effector cells were found to be predisposed toward becoming long-lived central memory cells during LCMV or other viral infections in mice (termed memory precursor effector cells [MPECs]). In contrast, cells expressing higher levels of CD57 and KLRG1 and reduced levels of IL-7R, CD28, and CD27 were found to be senescent, having reduced telomere length, proliferative capacity, and survival (termed short-lived effector T [Tsle] cells) (Kaech et al., 2003; Rutishauser and Kaech, 2010). Exactly when and how this long-lived memory versus short-lived effector cell fate decision is made has been the subject of intense study, leading to the identification of some of the factors and molecular mechanisms involved (Gerlach et al., 2011; Rutishauser and Kaech, 2010; Sallusto et al., 2004). However, we know much less about what determines which of the many different cytokines a given T cell is able to produce, whether the cell will be cytotoxic, or how this potential is related to its differentiation state or antigen specificity.

A number of ways to functionally characterize cytotoxic T cells have been developed over the years, including in vitro target cell lysis (Brunner et al., 1968), ELISPOT (Versteegen et al., 1988), intracellular staining for expression of cytotoxic granule components (such as granzymes and perforin) (Peters et al., 1991), staining of transiently exposed intravesicular CD107 molecules to probe for the cell's ability to secrete these components upon stimulation (Betts et al., 2003), and intracellular staining for expression of activation-induced cytokine production (Betts et al., 2006; De Rosa et al., 2004; Waldrop et al., 1997). The use of these techniques has revealed considerable heterogeneity in the functional capacity of CD8+ T cell populations and identified correlations between the extent of HIV-specific CD8+ T cell multifunctionality and the control of HIV viral load, suggesting a correlation between the diversity of T cell functionality and

the quality of the response (Betts et al., 2006; Makedonas and Betts, 2011; Seder et al., 2008). This correlation has also been observed in other systems such as *Leishmania*, adenovirus, and vaccinia virus vaccination (Darrah et al., 2007; Makedonas and Betts, 2011; Seder et al., 2008) and an antitumor response (Yuan et al., 2008). However, multifunctionality has also been shown to increase after antiretroviral therapy of HIV-infected individuals, suggesting that it may be a proxy for reduced antigen load rather than response quality (Rehr et al., 2008).

Although parallels have been drawn between multifunctionality and memory phenotypes (Rutishauser and Kaech, 2010; Sallusto et al., 2004), it is difficult to discern just how many distinct cellular phenotypes there are and how they are related to one another without the ability to look simultaneously at many phenotypic markers, functional capacity, and antigen specificity in individual cells. Flow cytometry has reached a practical limit of ~10–15 different parameters because of overlapping excitation and emmision spectra between different fluorophores, and thus new methods are needed. Particularly promising in this regard is the recently developed single-cell mass spectrometric (cytometry by time-of-flight or CyTOF) approach in which heavy metal isotopes are used to label antibodies and then labeled cells are analyzed by high throughput mass spectrometry to quantify 36 or more parameters at the single-cell level, with very little crosstalk between channels (Bendall et al., 2011; Ornatsky et al., 2006). Thus, to produce a more in-depth picture of CD8+ T cell diversity via CyTOF, we assembled a panel of 17 cell surface markers that are variably expressed on human CD8+ T cells. We also surveyed for the induction of nine functional attributes, including six intracellular cytokines, CD107 (a measure of degranulation), and two cytotoxic granule components, perforin and granzyme B, and devised a method for generating metal-labeled peptide-MHC tetramers for the identification of antigen-specific T cells. These data showed that there were more than 200 functional phenotypes represented by distinct CD8+ T cell subsets, a nearly combinatorial diversity out of the 512 possible combinations of these 9 attributes. Staining with tetramers representing specific viral epitopes for CMV, EBV, and influenza showed that T cells from each specificity expressed many of these functional attributes (80–100) and although there was some overlap in their responses, there were many that are unique. Furthermore, when we analyzed this data for the three principal components that account for the most variation (3D-PCA), we found a reproducible pattern of phenotypic diversity in all six healthy adults surveyed, which recapitulates and expands upon what is known about differentiation and maturation in these cells, showing a continuum with many hundreds of potential niches. In summary, we find that CD8+ T cells exhibit a much greater degree of phenotypic and functional complexity than previously appreciated and that virus-specific cells draw on this diversity in ways that are characteristic of the pathogen.

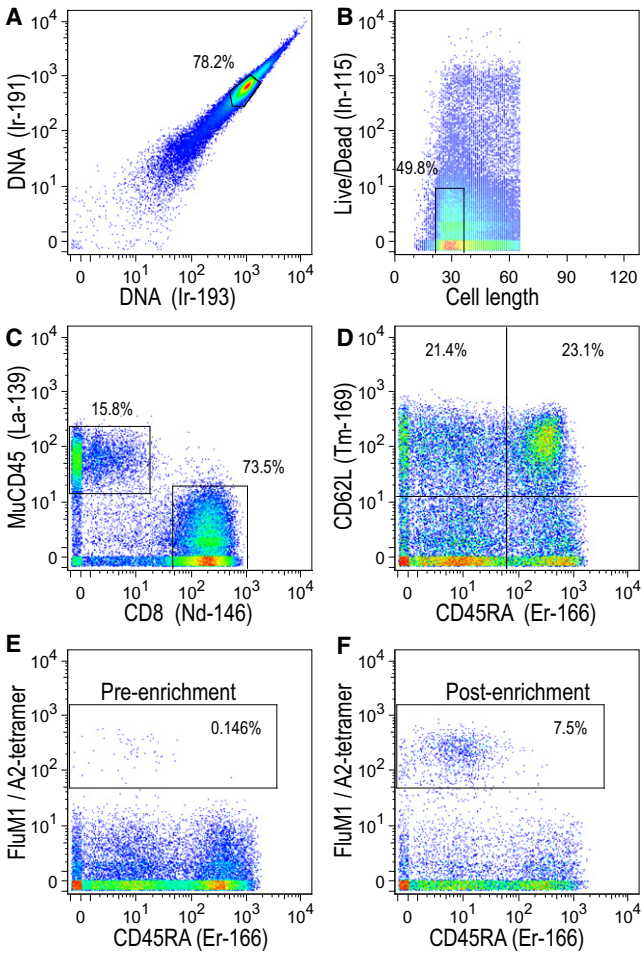

Figure 1. Representative Analysis of Antibody and pMHC Tetramer-Stained Cells via CyTOF

(A) Without light scatter to identify individual cells as in fluorescence flow cytomety, DNA content stained by an iridium-191/193 interchelator is used to identify individual cells.

(B) The cells are also gated for uniformity in the length of signal received by the ion detector and by exclusion of a live-dead viability stain (see Experimental Procedures).

(C and D) CD8+ T cells are distinguished from negative-control mouse cells stained with mouse CD45 (C), and two example surface stains (CD45RA versus CD62L) are shown (D).

(E and F) For the same donor sample, influenza-MP_{58-66}-HLA-A2 pMHC tetramer staining versus CD45RA staining are shown before (E) and after (F) tetramer enrichment via anti-c-*myc* magnetic particles (see Experimental Procedures).

The sample plotted here and in all figures is representative of six samples analyzed in this study. See also Figure S1.

RESULTS

Staining Panel Validation

After titrating antibody concentrations to optimize signal:noise for each marker, several approaches were taken to ensure that the antibodies used in this study maintained appropriate specificity. For several markers, such as CD45RA, CD45RO, CD27, CD62L, and CCR7, two-parameter dot-plot staining patterns consistent with those previously reported by fluorescence flow cytometry provided good evidence that these probes were reporting reliably (example in Figure 1). This strategy can also be employed more generally by looking at correlation matrices for all markers tested, where various surface and intracellular markers were correlated as expected from previous studies (not shown). Antibodies against inducible markers such as

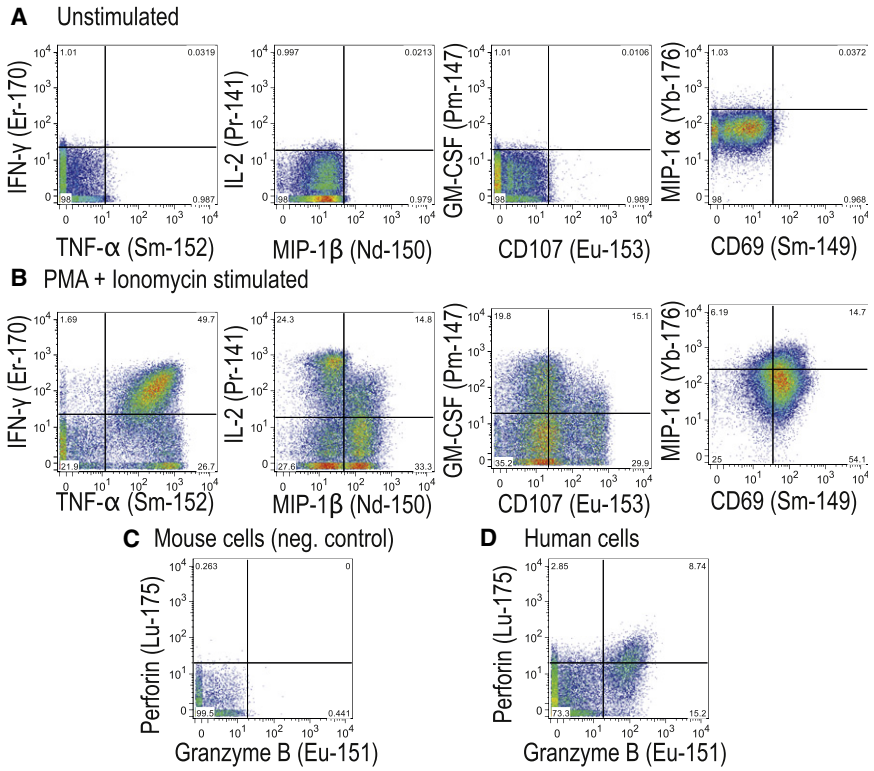

Figure 2. Boolean Gating for Functional Determination of Functional Capacity of Stimulated Live CD8+ T Cells

Boolean gates were set for each measure to define the multifunctional capacity of each stimulated cell.

(A) For inducible functions, not including perforin or granzyme B, the cut-off between positive and negative defined by the 99th percentile (1%+ cells) for unstimulated cells.

(B) PMA+ionomycin-stimulated cells are plotted for each of these functions.

(C and D) Spiked-in negative control mouse cells (C) were used to define the threshold of positivity for granzyme B and perforin of human CD8+ T cells (D).

intracellular cytokines CD69 and CD107 were validated by testing for appropriate increases upon stimulation (Figure 2; Figure S1 available online). Finally, mouse lymphocytes were added to each experimental sample prior to staining. These cells were distinguished by the addition of an anti-mouse CD45 marker to the panel (Figure 1). Because most of the human marker antibodies used in this study were generated in the mouse, very little background staining was observed for these cells (Figure S1). Sufficient signal:noise was an additional criterion for inclusion in the panel. In some cases, several commercial antibody clones were tested before identifying clones with sufficient signal as measured by mass spectrometry.

Phenotypic and Functional Assessment Strategy

After validating a phenotypic panel and creating CyTOF-compatible pMHC tetramer staining reagents and a tetramer-enrichment approach (described below), we needed a good way to measure all of these parameters simultaneously. PMA+ionomycin was used as a stimulus to elicit cytokine production and degranulation as a way to probe the functional capacity of each cell, while maintaining sufficient T cell receptor expression for subsequent peptide-MHC tetramer staining. For each donor, an unstimulated control sample was also included. After performing a stimulation time course (not shown), a 3 hr stimulus was used for all subsequent experiments. For consistency, all samples were frozen and thawed the day before stimulation allowing an overnight recovery period, which allowed for reinduction of CD62L expression that is lost after freeze-thaw (Costantini et al., 2003). To maintain the utility of CD62L expression as a phenotypic marker after stimulation, TAPI-2, a metalloproteinase inhibitor that prevents stimulation-induced cleavage of CD62L, was included in the media during stimulation (Jabbari and Harty, 2006). Both brefeldin A and monensin were included to prevent cytokine secretion and CD107 antibody degradation. We observed that this treatment also prevented upregulation of surface CD69 expression; however, probing CD69 intracellularly with the appropriate antibody clone (see Table S1) allowed us to detect substantial CD69 induction within the 3 hr stimulation time.

Principal Component Analysis

To handle the resulting large data sets, we employed principal component analysis (PCA) (Jackson, 1991), which is widely used to facilitate the visualization of multidimensional data (reviewed in Genser et al., 2007). For instance, it has been used to categorize gene expression profiles (Ringnér, 2008), to identify groups of human gut microbiota (Arumugam et al., 2011), to analyze the degree of helper T cell cytokine bias (Turner et al., 2003), and to analyze B cell phenotypic progression (Bendall et al., 2011). PCA works by taking data with a large number of parameters and deriving a smaller number of summary variables (principal components), which encapsulate most of the information of the original data so that it can be more readily displayed and interpreted. In contrast to clustering algorithms that group data into sets with similar properties and thus emphasize their commonality, the goal of PCA is to derive parameters that best describe (or explain) the variation in the entire data set. The effectiveness of this analysis can be quantified by calculating the relative amount of variation that each principle component describes (expressed as a percentage of the total variance; see Figure 3).

Here we used PCA as a way to distill the information from the 25 functional and phenotypic markers on PMA+ionomycin-stimulated T cells (see Experimental Procedures, Figure 3A). In this analysis, the first two principle components account for approximately 50% of the variation, and adding the third covers about 60% (Figure 3B). Additional variance can be explained by using additional principle components. However, their contribution was small (Figure 3B) and plots with components four through

A

Surface stains:	Atomic Mass:
6 pMHC tetramers	156,158,159,164,165,168
CD3	QDot = Cd-112 and others
CCR7	142
CD11a	148
CD7	143
CD8	146
CD27	154
CD28	160
CD29 (β1 integrin)	162
CD43	167
CD45RA	166
CD45RO	144
CD49d (VLA-4)	172
CD57	145
CD62L	169
KLRG1	174
HLA-DR	171
Intracellular stains:	**Atomic Mass:**
IL-2	141
GM-CSF	147
MIP-1α	176
MIP-1β	150
Granzyme B	151
CD69*	149
Perforin	175
TNF-α	152
IFN-γ	170
CD107a/b**	153
Other:	**Atomic Mass:**
DNA content	191, 193
"cell length"	N/A
Live/dead stain	115
Mouse CD45 ***	139

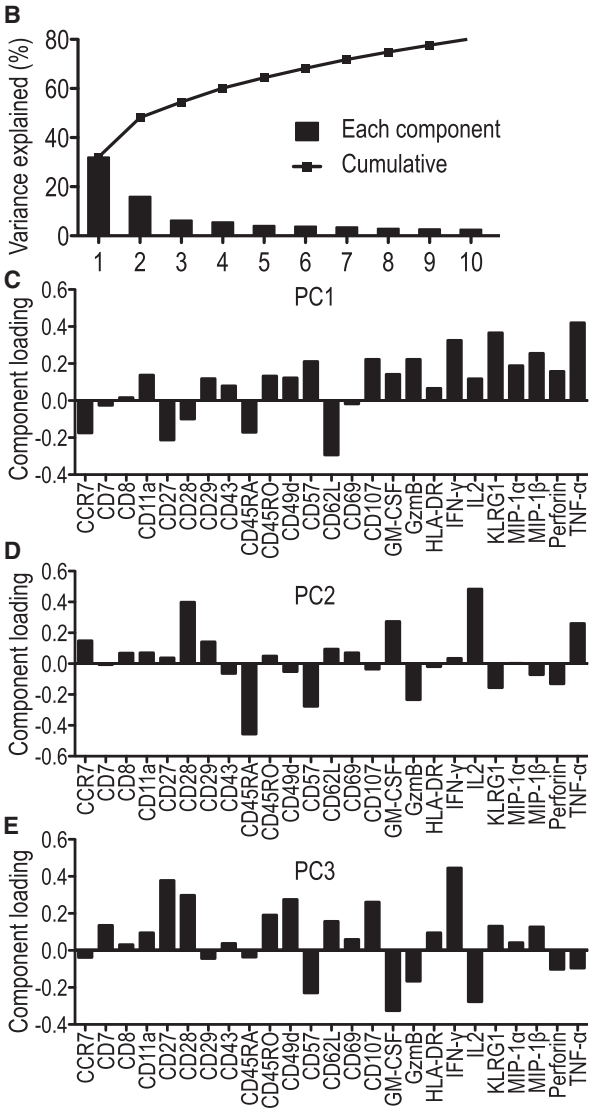

Figure 3. 36-Parameter Mass Cytometry Staining Experimental Setup and Principal Component Analysis

(A) A table of cellular markers and the atomic masses of each antibody or pMHC tetramer label are shown. To distill the information from 25 of these parameters, principal component analysis was used on live CD8+ T cells (gated as in Figure 1). *CD69 probed intracellularly, **anti-CD107a and -CD107b added at time of stimulation, ***anti-mouse CD45 used to distinguish negative control cells) (see Experimental Procedures).

(B) The percent variation explained are plotted for each component (bars) and cumulatively (line).

(C–E) The principle component analysis parameter loadings (weighting coefficients) for the first three components are plotted.

See also Figure S2.

six versus any of the first three components did not show any informative patterns (not shown). Therefore, we restricted our analysis to the first three components. Although this analysis is totally unsupervised, the apparent meaning of each component can be deduced based on previously defined CD8+ T cell subsets, with component 1 most closely tracking with the naive versus memory status of the cell, component 2 following the differentiation state, and component 3 mostly segregating variation within the central memory compartment (Figures 3C–3E). We then used the protein structure program PyMol (DeLano, 2002) to view these first three components in three dimensions, which enhances the ability to visualize the phenotypic complexity of the CD8+ T cell compartment. In particular, it revealed a folded Y-shaped pattern (Figure 4A; Movie S1 part 1), which we observed in all six subjects analyzed (Movie S1 part 2), with naive T cells at the base of the Y and short-lived effector cells and central memory cells forming distinct nodes at the tips of the Y. This pattern was robust, in that removing any one of the 25 parameters had no effect on its geometry (Figure S2).

To determine the composition of each of these major clusters, naive (CD45RA+ CD27+CD62L+CCR7+), central memory (Tcm, CD45RA−CD27+CD62L+CCR7+), effector memory (Tem, CD45RA−CD27− CD62L−CCR7−), and short-lived effector (Tsle, CD45RA+CD27−CD62L−CD28− KLRG1+CD57+) cells were gated based on stringent surface expression criteria and differentially colored on the PCA plot (Figure 4A; Movie S1 part 1). It is interesting to note the arrangement of these subsets, which suggests a continuum of phenotypes connecting the naive and memory subsets (and a continuum of memory cells connecting Tcm cells to Tem cells, which were then connected to Tsle cells). The phenotypic marker expression and functional capacities associated with this memory cell progression are illustrated in Figures 4B and 4C, showing progressive loss in functional markers associated with central memory phenotypes (such as CD62L, CCR7, and CD27) and gains in expression of markers associated with later stage memory cell differentiation and senescence (e.g., increased CD57 and granzyme B together with loss of CD28). Note a decline in CD107, IFN-γ, and TNF-α functional capacities at the end of this progression, indicative of functional exhaustion, whereas MIP-1β is maintained. The relationship between this phenotypic arrangement and cytokine or phenotypic markers can also be visualized by color-coding each cell by marker expression level (examples in Movie S1 parts 2 and 3) or by gating on selected populations (Figure S3, Movie S1 part 1). For instance, note that cells expressing the five major functions correlating with long-term nonprogression in HIV (Betts et al., 2006) were located within a small section of this phenotypic space within the Tem cell cluster (Figure S3). Also interesting is that the cells producing the most IL-2 were confined to the Tcm cell compartment (Figure S3, Movie S1 part 2) even though IL-2 production was not required to identify this subset of cells (Figure S2).

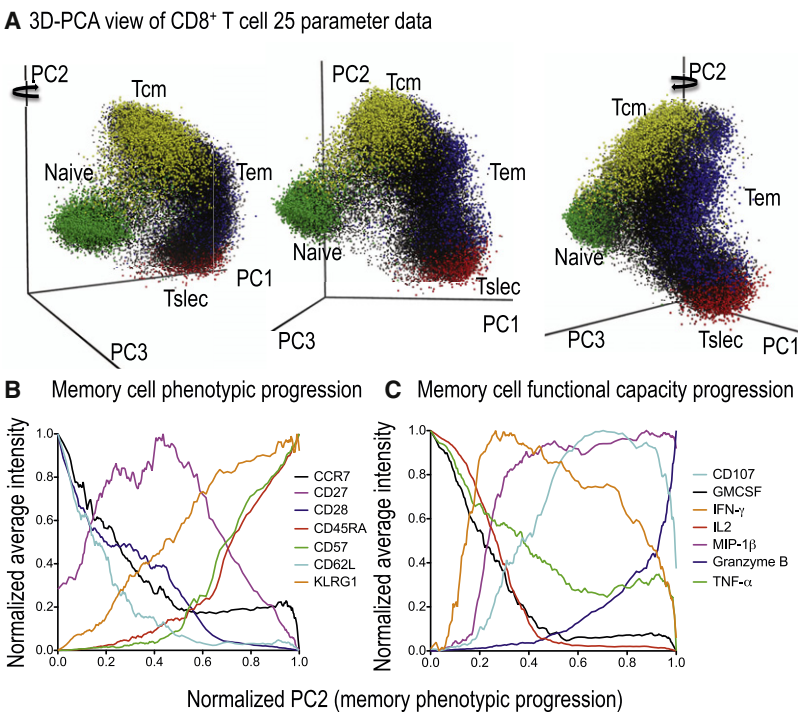

Figure 4. 3D-PCA Representation of CD8+ T Cell Data and Memory Cell Phenotypic and Functional Progression

(A) One cytometry data set is plotted on the first three principal component axes (a representative PMA+ ionomycin-stimulated CD8+ T cell sample) and shown from three different perspectives (rotated around the PC2-axis). After gating by surface marker phenotype, naive (green), central memory (Tcm, yellow), effector memory (Tem, blue), and short lived effector (Tslec, red) cell populations are overlaid to identify the main phenotypic clusters.

(B and C) To analyze only memory cells, cells in the principal components PC1 versus PC2 plot in (A) were gated to exclude the naive compartment (cells with low value for PC1) and subjected to further analysis. To determine the average expression for a number of different phenotypic markers and functional capacities across the entire range of PC2 values, small bins of cells with similar PC2 values were pooled and the average intensity of each marker was determined. These average expression for each phenotypic (B) and functional (C) parameters were normalized and plotted as a function of normalized PC2 values. In this way, the phenotypic progression of CD8+ memory T cells are represented by the *x* axis and the *y* axis represents the average expression of each marker.

See also Figure S3.

Unlike cluster analysis-based approaches, such as the SPADE approach (Bendall et al., 2011), no arbitrary groupings were made with 3D-PCA; instead, all cells were represented and the relationship between the phenotypes of each cell could be visualized on a single 2- or 3-dimensional plot. This serves the purpose of identifying major cell subsets without biases other than the choice of markers and to discern their overall characteristics and interrelatedness.

Combinatorial Diversity of Functional Capacity

We also analyzed these CD8+ T cells according to their functional capacity, which is the standard way in which subsets of effector T cells are defined. Here we ask whether CD8+ T cells fall into a limited number of cell types or are more diverse, as recently suggested (Ma et al., 2011). Thus we surveyed the expression of nine different functional attributes: six different cytokines, two cytotoxic granule components, and CD107, a degranulation marker in cells stimulated with PMA and ionomycin. We used Boolean gating to distinguish positives versus negatives for each of the cellular functions we measured. For seven functions, (TNF-α, interferon-γ, MIP-1α, MIP-1β, IL-2, GM-CSF, and CD107), the positive gate was defined by the 99th percentile intensity of unstimulated cells (Figure 2A). After stimulation with PMA+ionomycin (Figure 2B) or with anti-CD3±CD28 (not shown), significant increases in signal were observed for at least a subset of cells for all seven of these functions. For the expression of granzyme B and perforin, mouse cells were used as an internal negative control to delineate positive staining criteria (Figures 2C and 2D). For these 9 cellular functions, there were 512 possible combinations. Here we found that 151 distinct functional combinations could be found on cells that constitute at least 0.5% of the total and 242 when cells at frequencies at or above 0.1% were included (Figure 5A).

The use of anti-CD3 or anti-CD3+anti-CD28 as the stimuli reduced the number of functional variants to 97 and 129 (a 35% and 15% reduction in combinations occupied by >0.5% of the cells, respectively) (Figures 5A–5C), but revealed additional diversity when both phenotypic and functional data were considered by PCA (Figures 5D–5F). That is, new clusters of cells can be identified that have reduced responses in various functions when stimulated through CD3 compared to PMA+ionomycin, indicating an impairment in signal transduction. For instance, a large fraction of the terminally differentiated (PC2-low) cells have reduced functionality when stimulated by anti-CD3 or anti-CD3+anti-CD28, suggesting a role for TCR signaling defects in T cell exhaustion (see Figures S4 and S5). These differences may also be due to differences in signal transduction or cell death associated with stimulating with PMA+ionomycin compared to anti-CD3±anti-CD28. Indeed, cell death induced by TCR stimulation was influenced by T cell differentiation status (Russell et al., 1991). However, within a 3 hr stimulation, we do not expect that cell death is a major factor in these experiments. Another considerable fraction of cells, which overlap with the central memory compartment (PC2-high), showed a clear dependence on CD28 for cytokine production compared to later stage effectors (PC2-low), which were much less affected by CD28 stimulation. We conclude that CD8+ T lymphocytes are able to express a combinatorial diversity of effector molecules. We also expect that if we used additional functional markers, such as other cytokines and chemokines that CD8+ T cells produce, then we could see considerably more cell types.

To compare the functional potential of various subsets of cytotoxic T cells previously defined by surface marker expression, we performed the same analysis on cells gated by surface marker phenotype, as described above. Despite this stringent

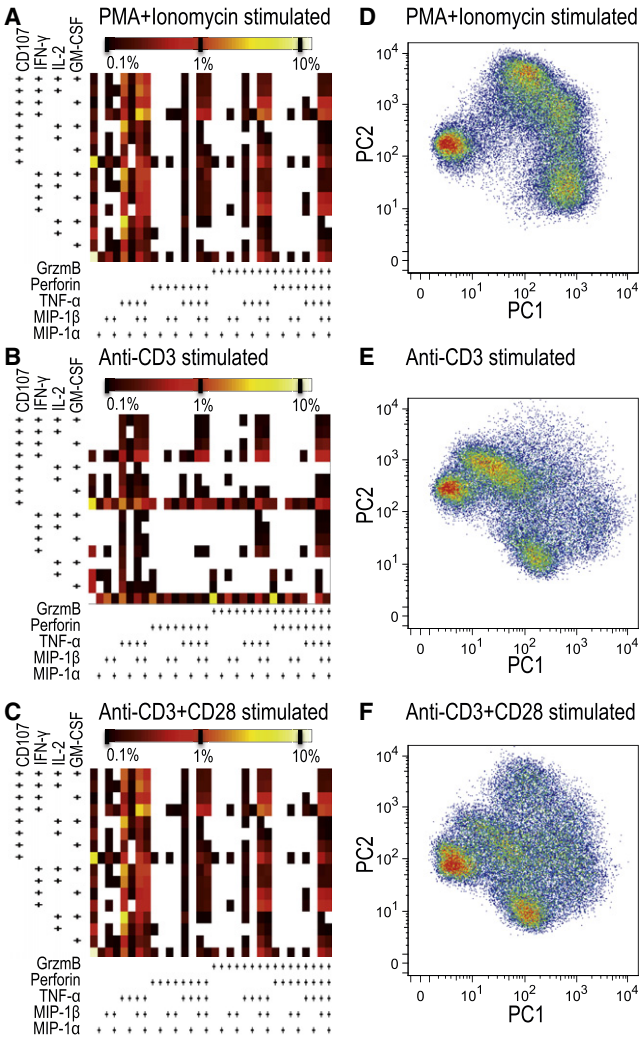

Figure 5. Functional and Phenotypic Analysis of CD8+ T Cells Stimulated by Various Means

(A–C) The combinatorial diversity of nine T cell functions were assessed in response to (A) PMA+ionomycin, (B) anti-CD3, or (C) anti-CD3+anti-CD28. $512 = 2^9$ possible functional phenotypes are each represented in a 16×32 grid, where the heat of each block represents the log scale frequency of cells displaying each combination of functional capacity (white represents frequencies below 0.1% cutoff).

(D–F) Psuedo-colored density-dot plots of the first two principal components after PCA loading with all 25 surface and intracellular parameters of PMA+ionomycin-stimulated cells (see Figure 3) are shown for cells stimulated with (D) PMA+ionomycin, (E) anti-CD3, and (F) anti-CD3+anti-CD28.

See also Figure S4.

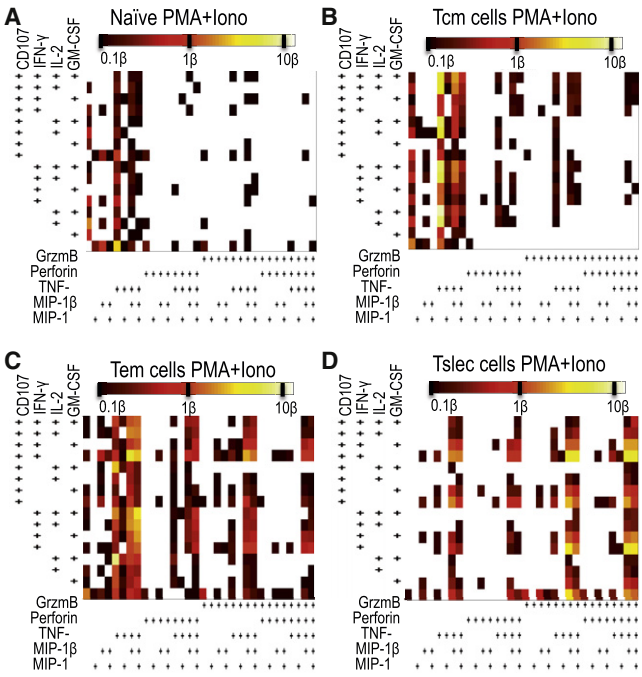

Figure 6. Diverse Combinatorial Functional Capacities of Stringently Defined CD8+ T Cell Subsets

As described for Figure 3, the combinatorial makeup of functional capcities are plotted on a 16×32 grid as a heat plot. PMA+ionomycin-stimulated live cells were further segregated based on stringent criteria: (A) naive ($CD45RA^+CD27^+CD62L^+CCR7^+$), (B) central memory (Tcm, $CD45RA^-CD27^+CD62L^+CCR7^+$), (C) effector memory (Tem, $CD45RA^-CD27^-CD62L^-CCR7^-$), and (D) short-lived effector (Tsle, $CD45RA^+CD27^-CD62L^-CD28^-KLRG1^+CD57^+$) cells before plotting frequencies of each the frequencies of cells expressing each combination of functional capacities.

See also Figure S5.

gating scheme, considerable diversity in functional capacity was observed in each cell subset (Figure 6).

Phenotypic and Functional Analysis of Virus-Specific Cells

The relevance to an immune response of these subsets can be further investigated by peptide-MHC tetramers (Altman et al., 1996), which label T cells according to their antigen specificity. To adapt the tetramer technique to CyTOF, we used a previously described streptavidin variant with C-terminal cysteines (Ramachandiran et al., 2007) that we labeled with chelators via maleimide chemistry and then added the particular metallic elements. To enable the efficient enrichment of tetramer-labeled T cells (Day et al., 2003), we also added a c-*myc* tag to the beta-2 microglobulin on the class I MHC molecules (Figures 1E and 1F). HLA-A2 and -B7 tetramers loaded with the appropriate peptides (see Experimental Procedures) were used to identify T cells specific for an influenza epitope (Figures 1E and 1F), several cytomegalovirus (CMV) epitopes (Figure S6), and several Epstein-Barr virus (EBV) epitopes (Figure S6). Analysis of the combinatorial diversity of functional capacity and 3D-PCA for these cells compared to the bulk $CD8^+$ T cell compartment highlights the fact that flu-, EBV-, and CMV-specific cells occupy distinct phenotypic and functional niches (Figure 7; Movie S1 part 4). For example, very few of the flu-specific TNF-α-producing cells also make MIP-1β compared to EBV- or CMV-specific cells, a smaller fraction of the CMV-specific cells make IL-2 compared to flu- or EBV-specific cells, and multifunctional flu-specific cells are skewed toward making GM-CSF at a higher frequency compared to the other specificities or the total $CD8^+$ lineage (Figures 7A–7C). With respect to the diversity of these functional attributes, antigen-specific cells are more focused

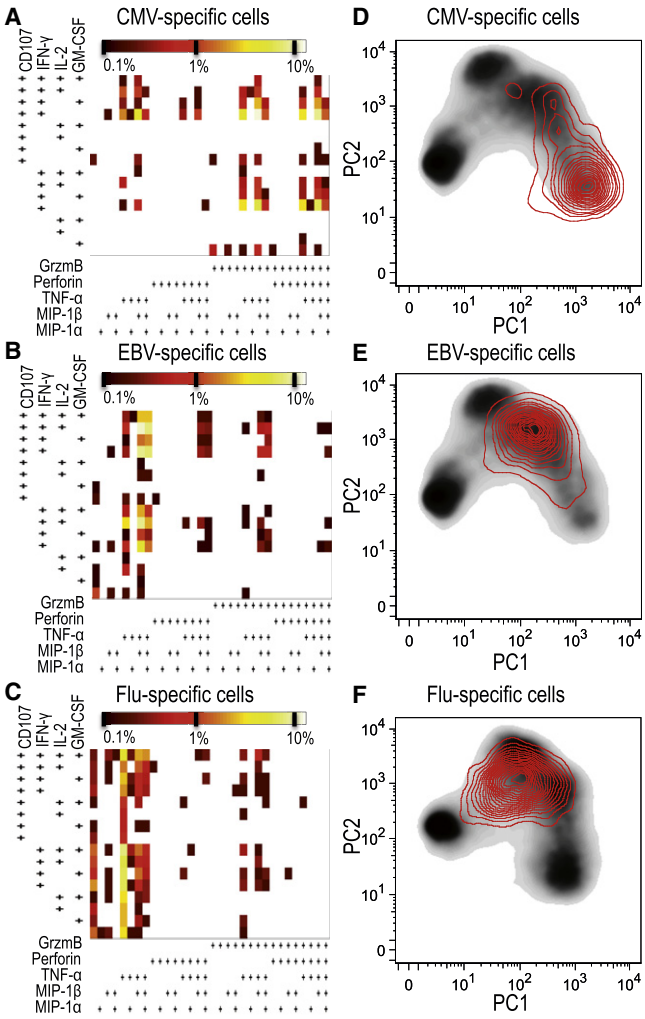

Figure 7. Functional and Phenotypic Analysis of Antigen-Specific CD8+ T Cells

(A–C) Examples of the combinatorial diversity in functional capacities of pMHC tetramer-stained cells are shown (as in Figure 2) for cells specific for CMV-pp65$_{482-490}$-HLA-A2 (A), EBV-BRLF$_{109-117}$-HLA-A2 (B), and influenza-MP$_{58-65}$-HLA-A2 (C).

(D–F) Density plots of the first two PCA components of total live PMA+-ionomycin-stimulated CD8+ T cells are overlaid with contour density plots of pMHC tetramer-positive cells in red for CMV- (D), EBV- (E), and influenza (F)-specific cells.

See also Figure S6.

compared to total CD8+ T cells, yet still produce 56–106 (depending on the specificity) combinations of functional markers (of the 512 possible).

These different phenotypes probably reflect the characteristics of the pathogen. Indeed, with some variation, most EBV-specific cells (a chronic infection) had Tem cell-like phenotypes (with some cells resembling late-stage effector [Tsle] cells in some individuals); in contrast, most flu-specific cells (an episodic infection) had Tcm cell-like phenotypes, and CMV-specific cells (a highly immunogenic chronic infection) had the functional properties of both late-stage effector and effectory memory cells (Figures 7D–7F), depending on the individual and epitope. However, not all of the functional capacities we observe can be easily explained by a simple differentiation scheme. For example, in instances where we could identify T cells specific for more than one epitope from the same virus (CMV or EBV) in the same individual, we found that the phenotypes and functional capacities of these T cells were often different, with some skewed toward later-stage effector phenotype and others more of a effector-memory phenotype (Figure S6). This skewing may be related to antigen expression patterns or to the epitope's placement within a dominance hierarchy (which has previously been shown to influence the relative contribution to protection from CMV infection) (Ouyang et al., 2003).

CMV-, EBV-, and Flu-Specific Cells Are Excluded from a Branch of Central Memory-like Cells

As described throughout this study, four major groups of cells were seen for PMA+ionomycin-stimulated CD8+ T cells as described by the first two principal components. When the third principal component was taken into account, we found additional variation within the central memory compartment at the tip of the folded "Y" (upper right of Figure 4A; Movie S1 part 4). None of the CMV-, EBV-, or flu-specific tetramers stain CD8+ T cells in this segment in any of the subjects tested. Further investigation into the defining features of this population revealed that CD49d-negative cells were also restricted to this compartment (CD49d-negative cells are also present in the naive cell cluster, not shown). CD49d (α4 integrin, VLA-4) is a component of a cell surface adhesion molecule involved in cellular trafficking. Thus, it is possible that all of the virus-specific cells being studied here are using this integrin for trafficking purposes. Although CD49d negativity is a striking feature of this subset, excluding CD49d from the analysis (as in Figure S2) does not eliminate this population, showing that it is not the only defining feature of this subset.

Another intriguing aspect of these data is that there is a large region of the Tcm cell compartment that is not populated by any of the virus-specific T cells. This compartment can be visualized by plotting PC2 versus PC3 after removing the naive cell compartment (not shown) or in the 3D-PCA visualization (Movie S1 part 4, this branch is highlighted by a white arrow).

DISCUSSION

We showed here that CyTOF technology can be used to characterize the phenotypic and functional complexity of a single type of lymphocyte, CD8+ T cells, to an unprecedented degree. We also showed that we can adapt peptide-MHC tetramer technology to this system for both identifying and enriching for antigen-specific T cells. Although the metal-labeled probes used here sometimes produced a lower signal compared to their fluorescent counterparts, this was more than made-up for by the lower background and the lack of crosstalk between labels.

A major goal of this study was to probe the relationships between surface marker phenotypes, functional capacities, and antigen specificities of cytotoxic T cells. Previous studies used surface marker correlates of functional, proliferative, and survival capacity to define naive, central memory, effector, and effector memory T cells (Hamann et al., 1997; Sallusto et al., 1999). Subsequent studies looking at a few more indicators at

a time have complicated this view and hypothesized that these subsets could be further segregated by taking additional markers into account such as the expression of costimulatory molecules CD27 and CD28 (Romero et al., 2007; Rufer et al., 2003), granule components, granzyme A, granzyme B, and perforin (Takata and Takiguchi, 2006), or other markers such as CD57 (Strioga et al., 2011) or KLRG-1 (Bengsch et al., 2010). Here we have probed all of these markers simultaneously and used 3D-PCA to generate an unbiased view of how these types of $CD8^+$ T cells are related to each other. Our approach also takes into account the functional capacity of each cell and allows for the fact that many of the markers being probed here are also expressed in a graded fashion. What we found, as discussed in more detail below, is that common definitions of naive, central memory, effector memory, and terminal effector subsets correspond to phenotypic clusters in our analysis. However, there are a range of cells with intermediate phenotypes that connect these clusters to form a continuum, which is especially apparent for memory cells. We also observe exceptional cells that fit classical definitions of a given subset, yet stray beyond the apparent bounds of the corresponding node in the 3D-PCA analyses. For instance, a small fraction of the cells that fit the classical definition of naive do not fall within the main naive cell cluster by PCA and may represent nonclassical memory cells, such as those recently described (Gattinoni et al., 2011).

One of the challenges of using this technology is to organize the data in an informative way with 25+ functional and phenotypic markers that we used here. The magnitude of this problem is seen in that whereas there are approximately 4,000 possible combinations of markers in a 12-color analysis, there are ~33,500,000 in a 25 color one (according to the formula $2^N - 1$). One way to display such large data sets is to use different forms of cluster analysis, and a variant of this called "SPADE" was recently used to interpret CyTOF data across the hematopoietic spectrum (Bendall et al., 2011). This works well to show relationships between different cell types and to postulate potential new cell subsets. A drawback of this approach is that it emphasizes the similarities between cells and that the assignment of distinct cell types is somewhat arbitrary. As an alternative, we used principal component analysis, which seeks to account for the variation in the data set (in this case, between individual $CD8^+$ cells) and combines the first three principal components into a 3D representation via a protein structure display program (PyMOL) (DeLano, 2002) that we call 3D-PCA. These first three PCA components account for nearly 60% of the variation of all markers probed and we find a common "folded Y" pattern in all six individuals analyzed. Because these were all healthy middle-aged adult aphaeresis donors, this pattern may change somewhat in younger and older individuals or if different antibody panels are used. Nonetheless, we observed a variably occupied yet remarkably common pattern for all donors tested, which has four general nodes that at least partially correspond to previously described general naive and memory subsets (Hamann et al., 1997; Sallusto et al., 1999). However, most strikingly, it also shows a graded progression between the subsets, especially within the memory compartment. As discussed above, some markers are expressed in a relatively binary fashion that would be expected to produce a punctate pattern with discrete nodes representing common phenotypes. However, with all 25 markers taken into account, there is a blending of phenotypes, suggesting that there is a stochastic expression of these binary markers as the cells progress. Alternatively, the markers that are graded in expression may be acting to smooth the borders between discrete subsets that would have been defined by the handful of binary markers.

Looking at just the memory compartment and using the second PCA principal component, we see a phenotypic progression connecting cells resembling central memory cells to cells resembling terminal effector cells displaying signs of functional exhaustion at the extreme of this progression. Based on this progression, which fits well with what we know about how $CD8^+$ T cells differentiate, we propose that principal component analysis used in this way can accurately define the differentiation state of a given cell and will be useful for identifying correlates of effective versus noneffective T cell-mediated immune responses. It may also offer better ways of accurately identifying "exhausted" T cells (Gallimore et al., 1998), which has sometimes proven difficult for human T cells (Duraiswamy et al., 2011).

Taking advantage of our ability to display the variation in three dimensions, we also observe an intriguingly diverging phenotype in the cells most closely resembling central memory T cells, which appears to represent a major bifurcation of $CD8^+$ T cell differentiation (see arrow in Movie S1 part 4). These cells have decreasing IL-2 expression and are negative for CD49d (the α4 integrin trafficking receptor subunit). It is also notable that none of the flu-, CMV-, or EBV-specific cells were present within this compartment. It will be interesting to further probe this diverging population of cells to determine their make-up in terms of specificity and function.

Because T cell subsets are best defined by their functional capacity and because multifunctionality is thought to be hallmark of T cells providing effective immunity to viruses and other pathogens (Betts et al., 2006; Makedonas and Betts, 2011; Seder et al., 2008), we took advantage of our ability to look at a large number of $CD8^+$ T cell functional capacities simultaneously. For each cell we used baseline or background measurements to delineate cells as positive or negative for 9 different functions, leading to 512 possible combinations of functional capacities. We saw that more than 200 of these combinations were used in substantial numbers. Although we could classify these $CD8^+$ T cells into more than 200 types and further describe each one, we prefer to use this data to make the general hypothesis that combinatorial diversity in functional capacity combined with diversity in surface marker phenotypes gives each $CD8^+$ T cell a nearly unique role that can be tailored to the needs of the immune response. We also saw that when cells were stringently gated by their surface marker phenotype, considerable diversity remained in the functional capacities of each memory subset. Not surprisingly, each subset was markedly skewed. For instance, stringently defined central memory cells used more functional combinations including IL-2 and GM-CSF, whereas late-stage effectors used more functional combinations including granzyme B and/or perforin. Furthermore, when we focus on antigen specificity by using peptide-MHC tetramers, the combinatorial functional capacity within each antigen specificity probed was again skewed yet remarkably diverse. This skewing toward specific functional niches for each of these viral

epitopes is most probably due the status of infection for each virus. Whereas EBV and CMV are chronic viral infections yielding ongoing responses of varying magnitude, it is likely that none of the healthy individuals tested had an active influenza infection, explaining the mostly central-memory-cell-like phenotype and combinatorial functional capacities of the flu-specific cells.

In summary, we have utilized the power of the CyTOF system to reexamine the functional and phenotypic diversity of human $CD8^+$ T lymphocytes. We have developed a visualization method, 3D-PCA, that robustly displays the phenotypic diversity of these lymphocytes in a distinct "folded Y" pattern, with the ends corresponding to known developmental stages (naive, etc.) and progression. This is significant because it shows that an unsupervised simultaneous analysis of 25 phenotypic and functional properties of human $CD8^+$ lymphocytes generally agrees with previous classification schemes but also shows how these subsets represent nodes on a continuum of T cell phenotypes. Our analyses also objectively describe a memory cell phenotypic progression involving progressive gains and losses of surface markers and phenotypic capacities (both predictable and unpredictable), which we think is important for objectively defining the degree of T cell differentiation and exhaustion. By focusing specifically on nine known functional attributes, we also find that these are distributed in an almost random combinatorial manner, with more than 100 of a possible 512 combinations being used in significant numbers of cells (>.5%) and more than twice that if the stringency is lower. Many these combinations are expressed in viral epitope-specific T cells, as identified by peptide-MHC tetramer staining, showing that they are actively utilized, with different viral responses favoring different combinations. These data show that cytokine usage in $CD8^+$ T lymphocytes is not confined to a limited number of distinct subsets, but rather is much broader and combinatorial in nature, allowing a great deal of flexibility in orchestrating an effective pathogen response. Lastly, these data also show the power of the CyTOF technology to enhance our understanding of and ability to analyze T cell responses in all their complexity.

EXPERIMENTAL PROCEDURES

Cells

Leukocyte reduction system cones (LRS) containing peripheral blood mononuclear cells (from platelet aphaeresis donors) were obtained from the Stanford Blood Center according to IRB protocol. For the purposes of pMHC tetramer staining experiments, HLA-A2 or -B7 positive donor samples were typed and identified by the Stanford Blood Center. These samples were also serotyped for cytomegalovirus (CMV) infection status. For $CD8^+$ enrichment by negative selection, the LRS samples were diluted to 20 ml phosphate-buffered saline (PBS) + 2% fetal calf serum before adding 750 μl of $CD8^+$-T cell RosetteSep cocktail (StemCell Technologies). The cells were further diluted with PBS + 2% fetal calf serum and ficoll-separated (Ficoll-Paque PLUS, GE Healthcare) from red blood cells and negatively selected cells before cryopreservation in 90% fetal calf serum + 10% DMSO. All samples were processed, $CD8^+$ T cell enriched, and frozen prior to use.

Stimulation, Staining, and Data Acquisition

Cyropreserved cells were thawed and washed with complete RPMI before overnight recovery at 37°C. After recovery, the cells were ficoll density separated to remove dead cells prior to stimulation. For stimulation, all cells were cultured for 3 hr at approximately 15×10^6/ml in complete RPMI (10% fetal calf serum) plus 1× brefeldin A (eBioscience), 1× monensin (eBioscience), 2.5 μg/ml anti-CD107a, 1.25 μg/ml anti-CD107b (see Table S1), and 10 μM TAPI-2 (VWR International). For PMA+ionomycin stimulation, 150 ng/ml PMA + 1 μM ionomycin were added to the cells. For CD3 ± CD28 antibody stimulation, 100 μl of 1 μg/ml OKT3 anti-CD3 ± 5 μg/ml CD28.2 anti-CD28 (low endotoxin azide free format, Biolegend) were added to each well of NUNC 96-well ELISA plates in PBS and incubated at 4°C overnight before washing 3× with complete RPMI to block before addition of cells at 1.5×10^6 cells per well.

At the end of the 3 hr stimulation, cells were pipetted vigorously to remove adherent cells from the plate. At this point, 5×10^5 negative-control mouse red blood cell-depleted splenocytes were added to each condition. These cells serve as an internal control for nonspecific binding for all stains. These negative control cells also serve to ensure that cell doublets or other erroneous sources of crosstalk were not part of the analysis. These problems were apparent only in some preliminary experiments (cell acquisition rate too high, etc.); thus, this control was included but not critical for all experiments shown here.

The combined stimulated human and control mouse cells were transferred to 96-well plates (or tubes), washed, and resuspended in cytometry buffer (PBS + 0.05% sodium azide + 2 mM EDTA + 2% fetal calf serum). The cells were then stained for 1 hr at room temperature at a cell density up to 3×10^8/ml with approximately 100 nM pMHC tetramer and purified 5 μg/ml anti-CD16 + 5 μg/ml anti-CD32 to reduce nonspecific binding (BD Biosciences)—in some cases 20 μM desatinib (Sigma/Aldrich) was added to improve tetramer staining (Lissina et al., 2009). After tetramer staining, the cells were transferred to ice for the duration of the staining. For tetramer enrichment, a sample of cells was taken for the pre-enriched fraction, and the rest of the cells were washed twice in cytomety buffer and stained with 30% v/v anti-myc particles (Miltenyi Biotec) for 20 min on ice. The cells were then washed and applied to an LS size MACS enrichment column (Miltenyi Biotec), washed with 5 ml of cytometry buffer, and eluted with 5 ml cytometry buffer after removing the column from the magnetic field. Pre-enriched and tetramer-enriched cells were then stained for 30 min on ice with a prepared cocktail of metal-conjugated surface-marker antibodies at concentrations found to be effective in prior antibody tests (see Table S1 for a list of antibodies used). After surface staining, cells were washed 1× and resuspended in 20 μM indium-115-loaded maleimido-mono-amine-DOTA in PBS (a sulfhydryl reactive trivalent cation chelating bifunctional ligand, Macrocyclics #B-272, mixed with 0.5 molar ratio of 115-indium chloride and stock solution dissolved in DVS "L-buffer" [DVS Sciences] at 1 mM, stable at 4°C and working much like commercially available amine-reactive Live/Dead staining reagents, Invitrogen). After 30 min on ice, the cells were washed 3× in cytometry buffer and resuspended in PBS + 2% paraformade (Electron Microscopy Sciences). After overnight fixation at 4°C, the cells were washed 2× in 1× intracellular staining permeablization buffer (eBioscience, Cat. 00-8333-56) and stained with a cocktail of intracellular antibodies (Table S1) on ice for 45 min, washed 2× in cytometry buffer, and labeled for 20 min at room temperature with 250 nM iridium interchelator (DVS Sciences) suspended in PBS + 2% paraformaldehyde.

Finally, the cells were washed 2× in cytometry buffer, 2× in PBS, and 2× in distilled water before diluting to the appropriate concentration to achieve an acquisition rate <500 events/s on the CyTOF instrument. CyTOF data were acquired and analyzed on the fly, using dual-count mode (calibrated on the fly, combining pulse-count and intensity information) with noise-reduction mode turned off. All other settings were either default settings or optimized with tuning solution as instructed by DVS sciences. For cells that had undetectable levels of a given isotope (a zero value for a given parameter), the default setting on the software assigns these cells a random value between 0 and −1, creating a square distribution between 0 and −1. This makes histogram plots more manageable, maintaining an ability to appreciate the number of cells in the zero bins. This effect can be seen both in histograms and in density dot plots used in this study. It also has negligible or no effect on subsequent PCA or Boolean analyses.

Antibody Labeling

Purified antibodies (lacking carrier proteins) were purchased from the companies listed in Table S1. The antibodies were labeled 100 μg at a time according to instructions provided by DVS Sciences with heavy metal-preloaded maleimide-coupled MAXPAR chelating polymers via the "Pre-Load Method v1.1."

pMHC Tetramer Production

To produce the various biotinylated pMHC molecules, HLA-A*0201 or HLA-B*0702 was refolded with a UV-cleavable peptide, biotinylated, and purified as described (Bakker et al., 2008; Toebes et al., 2006). After purification, the protein stock was stored in PBS + 50% glycerol at −20°C. For each peptide specificity, peptide exchange reactions were set up in 100 μl volumes, each containing 10 μM peptide and 100 μg/ml HLA-A2 or HLA-B7 protein in PBS. Peptide sequences used in this study were as follows. For HLA-A2: CMV, $pp65_{482-490}$, NLVPMVATV, $FluM1/MP_{58-66}$, GILGFVFTL, Mart1 (altered Melan-A_{26-35} A27L) (Sliz et al., 2001) ELAGIGILTV, GLCTLVAML, EBV-$BRLF1_{109-117}$, YVLDHLIVV, EBV-$BMLF1_{259-267}$, GLCTLVAML; for HLA-B7: CMV2, $pp65_{265-275}$, RPHERNGFTVL, CMV3, $pp65_{417-426}$, TPRVTGGGAM, EBV-$EBNA3A_{379-387}$, RPPIFIRRL. After a 20 min exposure to 365 nm UV irradiation with a Stratagene UV Stratalinker 2400, the protein was stored at 4°C overnight to complete the exchange. After overnight incubation to complete the peptide exchange, the protein was transferred to a tube for tetramerization by step-wise (>4 additions with 5 min incubations at room temperature between) addition of streptavidin to final 1:4 molar ratio.

Streptavidin Expression and Heavy Metal Labeling

Cysteine residues were introduced to the C terminus of streptavidin prior to recombinant expression, refolding, and purification as described (Ramachandiran et al., 2007). After purification by size-exclusion chromatography, the protein was stored in 10 mM DTT in 20 mM HEPES (pH 7.2)-buffered saline and 50% glycerol before coupling. For heavy metal coupling, the protein was exchanged into 1 M NaCl, 500 mM HEPES (pH 7.2), 1 mM TCEP reducing agent, 10 mM EDTA, and 20 mM NaOH (streptavidin coupling buffer). 5 μl of heavy metal solution (DVS Sciences) was added to 20 μl streptavidin-coupling buffer and incubated at room temperature until most/all precipitation dissolved. 10 μl of protein in streptavidin-coupling buffer at 2.5 mg/ml was added to 1 vial of MAXPAR chelating polymer (25 μg streptavidin added to 0.2 mg of polymer), then the 25 μl metal solution was added to the same tube and incubated at room temperature overnight. The next day, the protein was exchanged into 20 mM HEPES (pH 7.2)-buffered saline with a 30 kDa cutoff protein concentrator (Millipore).

Data Analysis

After built-in cell-identifying software creates an FCS file, mass cytometry data can be analyzed in a manner very similar to standard flow cytometry data by FlowJo software (Treestar, Inc.). As has been described (Bendall et al., 2011; Ornatsky et al., 2006), light scatter cannot be used to identify cell events by mass spectroscopy. Instead, DNA content and the "cell length" (indicative of the length in the burst of signal that is detected as cells pass through the plasma torch) parameters can be used to identify single-cell events. Next, the cells were gated on live CD8+ T cells with a heavy-metal-labeled cell-viability marker and a heavy-metal-labeled CD8 antibody (see Figure 1). These events were exported to a tab-delimited text file with FlowJo v9.1 or v9.3.2 and further analyzed with scripts written in Matlab. In some cases the Matlab scripts produced text files containing additional principal componenent analysis parameters that were converted back to FCS files with a custom algorithm written in Java (generously provided by W. Moore). In other instances, the Matlab scripts produced pdb files read by PyMOL software (DeLano Scientific LLC) to produce quicktime movie files.

All Matlab scripts started with transformation of data into logicle biexponential scaling as described (Parks et al., 2006) (also to allow comparison with FlowJo, which also used the logicle display method). Several functions were used. A correlation matrix heat-plot function based on the Matlab "corrcoef" function, a clustergram function based on the "clustergram" function, a principal component analysis function based on the Matlab "princomp" function that rescales the results for display and further analysis in FlowJo or PyMol, and a custom Boolean gating function for plotting the combinatorial expression of nine different T cell functions plotted as a 16×32 log scale frequency heat-plot.

SUPPLEMENTAL INFORMATION

Supplemental Information includes six figures, one table (of all antibody clones and references for each), and one movie and can be found with this article online at doi:10.1016/j.immuni.2012.01.002.

ACKNOWLEDGMENTS

The authors would like to thank D. Parks and W. Moore for helpful discussions and help with FlowJo and FCS files, P. Lund for helpful discussions and a T cell stimulation protocol, M. Leipold for help with CyTOF machine maintenance, E. Zunder, B. Bodenmiller, and E. Simonds for general help with CyTOF usage, and A. Han, B. Kidd, W. O'Gorman, O. Goldberger, and Y.-h. Chien for helpful discussions. This work was supported by NIH grants U19-AI057229 and U19-AI090019, Bill and Melinda Gates Foundation Grand Challenges Exploration phase I and II grants, and The Howard Hughes Medical Institute. E.W.N. is supported by The American Cancer Society's Steven Stanley and Edward Albert Bielfelt Post-Doctoral Fellowship. S.C.B. is supported by a Damon Runyon Postdoctoral Fellowship (DRG-2017-09). G.P.N. is supported by an endowed chair from Rachtford and Carlota A. Harris. G.P.N. is a paid consultant for Becton Dickinson Biosciences, a member of the Board of Directors and consultant for DVS Sciences, and has equity holdings in DVS Biosciences.

Received: September 3, 2011
Revised: October 19, 2011
Accepted: November 29, 2011
Published online: January 19, 2012

REFERENCES

Altman, J.D., Moss, P.A., Goulder, P.J., Barouch, D.H., McHeyzer-Williams, M.G., Bell, J.I., McMichael, A.J., and Davis, M.M. (1996). Phenotypic analysis of antigen-specific T lymphocytes. Science *274*, 94–96.

Arumugam, M., Raes, J., Pelletier, E., Le Paslier, D., Yamada, T., Mende, D.R., Fernandes, G.R., Tap, J., Bruls, T., Batto, J.M., et al; MetaHIT Consortium. (2011). Enterotypes of the human gut microbiome. Nature *473*, 174–180.

Bakker, A.H., Hoppes, R., Linnemann, C., Toebes, M., Rodenko, B., Berkers, C.R., Hadrup, S.R., van Esch, W.J., Heemskerk, M.H., Ovaa, H., and Schumacher, T.N. (2008). Conditional MHC class I ligands and peptide exchange technology for the human MHC gene products HLA-A1, -A3, -A11, and -B7. Proc. Natl. Acad. Sci. USA *105*, 3825–3830.

Bendall, S.C., Simonds, E.F., Qiu, P., Amir, A.D., Krutzik, P.O., Finck, R., Bruggner, R.V., Melamed, R., Trejo, A., Ornatsky, O.I., et al. (2011). Single-cell mass cytometry of differential immune and drug responses across a human hematopoietic continuum. Science *332*, 687–696.

Bengsch, B., Seigel, B., Ruhl, M., Timm, J., Kuntz, M., Blum, H.E., Pircher, H., and Thimme, R. (2010). Coexpression of PD-1, 2B4, CD160 and KLRG1 on exhausted HCV-specific CD8+ T cells is linked to antigen recognition and T cell differentiation. PLoS Pathog. *6*, e1000947.

Betts, M.R., Brenchley, J.M., Price, D.A., De Rosa, S.C., Douek, D.C., Roederer, M., and Koup, R.A. (2003). Sensitive and viable identification of antigen-specific CD8+ T cells by a flow cytometric assay for degranulation. J. Immunol. Methods *281*, 65–78.

Betts, M.R., Nason, M.C., West, S.M., De Rosa, S.C., Migueles, S.A., Abraham, J., Lederman, M.M., Benito, J.M., Goepfert, P.A., Connors, M., et al. (2006). HIV nonprogressors preferentially maintain highly functional HIV-specific CD8+ T cells. Blood *107*, 4781–4789.

Brunner, K.T., Mauel, J., Cerottini, J.C., and Chapuis, B. (1968). Quantitative assay of the lytic action of immune lymphoid cells on 51-Cr-labelled allogeneic target cells in vitro; inhibition by isoantibody and by drugs. Immunology *14*, 181–196.

Costantini, A., Mancini, S., Giuliodoro, S., Butini, L., Regnery, C.M., Silvestri, G., and Montroni, M. (2003). Effects of cryopreservation on lymphocyte immunophenotype and function. J. Immunol. Methods *278*, 145–155.

Darrah, P.A., Patel, D.T., De Luca, P.M., Lindsay, R.W., Davey, D.F., Flynn, B.J., Hoff, S.T., Andersen, P., Reed, S.G., Morris, S.L., et al. (2007). Multifunctional TH1 cells define a correlate of vaccine-mediated protection against *Leishmania major*. Nat. Med. *13*, 843–850.

Davis, M.M., Altman, J.D., and Newell, E.W. (2011). Interrogating the repertoire: broadening the scope of peptide-MHC multimer analysis. Nat. Rev. Immunol. *11*, 551–558.

Day, C.L., Seth, N.P., Lucas, M., Appel, H., Gauthier, L., Lauer, G.M., Robbins, G.K., Szczepiorkowski, Z.M., Casson, D.R., Chung, R.T., et al. (2003). Ex vivo analysis of human memory CD4 T cells specific for hepatitis C virus using MHC class II tetramers. J. Clin. Invest. *112*, 831–842.

De Rosa, S.C., Lu, F.X., Yu, J., Perfetto, S.P., Falloon, J., Moser, S., Evans, T.G., Koup, R., Miller, C.J., and Roederer, M. (2004). Vaccination in humans generates broad T cell cytokine responses. J. Immunol. *173*, 5372–5380.

DeLano, W.L. (2002). The PyMOL User's Manual (San Carlos, CA: DeLano Scientific).

Duraiswamy, J., Ibegbu, C.C., Masopust, D., Miller, J.D., Araki, K., Doho, G.H., Tata, P., Gupta, S., Zilliox, M.J., Nakaya, H.I., et al. (2011). Phenotype, function, and gene expression profiles of programmed death-1(hi) CD8 T cells in healthy human adults. J. Immunol. *186*, 4200–4212.

Gallimore, A., Glithero, A., Godkin, A., Tissot, A.C., Plückthun, A., Elliott, T., Hengartner, H., and Zinkernagel, R. (1998). Induction and exhaustion of lymphocytic choriomeningitis virus-specific cytotoxic T lymphocytes visualized using soluble tetrameric major histocompatibility complex class I-peptide complexes. J. Exp. Med. *187*, 1383–1393.

Gattinoni, L., Lugli, E., Ji, Y., Pos, Z., Paulos, C.M., Quigley, M.F., Almeida, J.R., Gostick, E., Yu, Z., Carpenito, C., et al. (2011). A human memory T cell subset with stem cell-like properties. Nat. Med. *17*, 1290–1297.

Genser, B., Cooper, P.J., Yazdanbakhsh, M., Barreto, M.L., and Rodrigues, L.C. (2007). A guide to modern statistical analysis of immunological data. BMC Immunol. *8*, 27.

Gerlach, C., van Heijst, J.W., and Schumacher, T.N. (2011). The descent of memory T cells. Ann. N Y Acad. Sci. *1217*, 139–153.

Hamann, D., Baars, P.A., Rep, M.H., Hooibrink, B., Kerkhof-Garde, S.R., Klein, M.R., and van Lier, R.A. (1997). Phenotypic and functional separation of memory and effector human CD8+ T cells. J. Exp. Med. *186*, 1407–1418.

Jabbari, A., and Harty, J.T. (2006). Simultaneous assessment of antigen-stimulated cytokine production and memory subset composition of memory CD8 T cells. J. Immunol. Methods *313*, 161–168.

Jackson, J.E. (1991). PCA with more than two variables. In User's Guide to Principal Compoenent Analysis, J.E. Jackson, ed. (New York: John Wiley and Sons), pp. 26–62.

Kaech, S.M., Tan, J.T., Wherry, E.J., Konieczny, B.T., Surh, C.D., and Ahmed, R. (2003). Selective expression of the interleukin 7 receptor identifies effector CD8 T cells that give rise to long-lived memory cells. Nat. Immunol. *4*, 1191–1198.

Lissina, A., Ladell, K., Skowera, A., Clement, M., Edwards, E., Seggewiss, R., van den Berg, H.A., Gostick, E., Gallagher, K., Jones, E., et al. (2009). Protein kinase inhibitors substantially improve the physical detection of T-cells with peptide-MHC tetramers. J. Immunol. Methods *340*, 11–24.

Ma, C., Fan, R., Ahmad, H., Shi, Q., Comin-Anduix, B., Chodon, T., Koya, R.C., Liu, C.C., Kwong, G.A., Radu, C.G., et al. (2011). A clinical microchip for evaluation of single immune cells reveals high functional heterogeneity in phenotypically similar T cells. Nat. Med. *17*, 738–743.

Makedonas, G., and Betts, M.R. (2011). Living in a house of cards: re-evaluating CD8+ T-cell immune correlates against HIV. Immunol. Rev. *239*, 109–124.

Ornatsky, O., Baranov, V.I., Bandura, D.R., Tanner, S.D., and Dick, J. (2006). Multiple cellular antigen detection by ICP-MS. J. Immunol. Methods *308*, 68–76.

Ouyang, Q., Wagner, W.M., Wikby, A., Walter, S., Aubert, G., Dodi, A.I., Travers, P., and Pawelec, G. (2003). Large numbers of dysfunctional CD8+ T lymphocytes bearing receptors for a single dominant CMV epitope in the very old. J. Clin. Immunol. *23*, 247–257.

Parks, D.R., Roederer, M., and Moore, W.A. (2006). A new "Logicle" display method avoids deceptive effects of logarithmic scaling for low signals and compensated data. Cytometry A *69*, 541–551.

Peters, P.J., Borst, J., Oorschot, V., Fukuda, M., Krähenbühl, O., Tschopp, J., Slot, J.W., and Geuze, H.J. (1991). Cytotoxic T lymphocyte granules are secretory lysosomes, containing both perforin and granzymes. J. Exp. Med. *173*, 1099–1109.

Ramachandiran, V., Grigoriev, V., Lan, L., Ravkov, E., Mertens, S.A., and Altman, J.D. (2007). A robust method for production of MHC tetramers with small molecule fluorophores. J. Immunol. Methods *319*, 13–20.

Rehr, M., Cahenzli, J., Haas, A., Price, D.A., Gostick, E., Huber, M., Karrer, U., and Oxenius, A. (2008). Emergence of polyfunctional CD8+ T cells after prolonged suppression of human immunodeficiency virus replication by antiretroviral therapy. J. Virol. *82*, 3391–3404.

Ringnér, M. (2008). What is principal component analysis? Nat. Biotechnol. *26*, 303–304.

Romero, P., Zippelius, A., Kurth, I., Pittet, M.J., Touvrey, C., Iancu, E.M., Corthesy, P., Devevre, E., Speiser, D.E., and Rufer, N. (2007). Four functionally distinct populations of human effector-memory CD8+ T lymphocytes. J. Immunol. *178*, 4112–4119.

Rufer, N., Zippelius, A., Batard, P., Pittet, M.J., Kurth, I., Corthesy, P., Cerottini, J.C., Leyvraz, S., Roosnek, E., Nabholz, M., and Romero, P. (2003). Ex vivo characterization of human CD8+ T subsets with distinct replicative history and partial effector functions. Blood *102*, 1779–1787.

Russell, J.H., White, C.L., Loh, D.Y., and Meleedy-Rey, P. (1991). Receptor-stimulated death pathway is opened by antigen in mature T cells. Proc. Natl. Acad. Sci. USA *88*, 2151–2155.

Rutishauser, R.L., and Kaech, S.M. (2010). Generating diversity: transcriptional regulation of effector and memory CD8 T-cell differentiation. Immunol. Rev. *235*, 219–233.

Sallusto, F., Lenig, D., Förster, R., Lipp, M., and Lanzavecchia, A. (1999). Two subsets of memory T lymphocytes with distinct homing potentials and effector functions. Nature *401*, 708–712.

Sallusto, F., Geginat, J., and Lanzavecchia, A. (2004). Central memory and effector memory T cell subsets: function, generation, and maintenance. Annu. Rev. Immunol. *22*, 745–763.

Seder, R.A., Darrah, P.A., and Roederer, M. (2008). T-cell quality in memory and protection: implications for vaccine design. Nat. Rev. Immunol. *8*, 247–258.

Sliz, P., Michielin, O., Cerottini, J.C., Luescher, I., Romero, P., Karplus, M., and Wiley, D.C. (2001). Crystal structures of two closely related but antigenically distinct HLA-A2/melanocyte-melanoma tumor-antigen peptide complexes. J. Immunol. *167*, 3276–3284.

Strioga, M., Pasukoniene, V., and Characiejus, D. (2011). CD8+ CD28- and CD8+ CD57+ T cells and their role in health and disease. Immunology *134*, 17–32.

Takata, H., and Takiguchi, M. (2006). Three memory subsets of human CD8+ T cells differently expressing three cytolytic effector molecules. J. Immunol. *177*, 4330–4340.

Toebes, M., Coccoris, M., Bins, A., Rodenko, B., Gomez, R., Nieuwkoop, N.J., van de Kasteele, W., Rimmelzwaan, G.F., Haanen, J.B., Ovaa, H., and Schumacher, T.N. (2006). Design and use of conditional MHC class I ligands. Nat. Med. *12*, 246–251.

Turner, J.D., Faulkner, H., Kamgno, J., Cormont, F., Van Snick, J., Else, K.J., Grencis, R.K., Behnke, J.M., Boussinesq, M., and Bradley, J.E. (2003). Th2 cytokines are associated with reduced worm burdens in a human intestinal helminth infection. J. Infect. Dis. *188*, 1768–1775.

Versteegen, J.M., Logtenberg, T., and Ballieux, R.E. (1988). Enumeration of IFN-gamma-producing human lymphocytes by spot-ELISA. A method to detect lymphokine-producing lymphocytes at the single-cell level. J. Immunol. Methods *111*, 25–29.

Waldrop, S.L., Pitcher, C.J., Peterson, D.M., Maino, V.C., and Picker, L.J. (1997). Determination of antigen-specific memory/effector CD4+ T cell frequencies by flow cytometry: evidence for a novel, antigen-specific homeostatic mechanism in HIV-associated immunodeficiency. J. Clin. Invest. *99*, 1739–1750.

Yuan, J., Gnjatic, S., Li, H., Powel, S., Gallardo, H.F., Ritter, E., Ku, G.Y., Jungbluth, A.A., Segal, N.H., Rasalan, T.S., et al. (2008). CTLA-4 blockade enhances polyfunctional NY-ESO-1 specific T cell responses in metastatic melanoma patients with clinical benefit. Proc. Natl. Acad. Sci. USA *105*, 20410–20415.